Title

Manganese oxidation as the origin of the anomalous capacity of Mn-containing Li-excess cathode materials

Authors

Radin, Maxwell D
Vinckeviciute, Julija
Seshadri, Ram
et al.

Publication Date

2019-07-29

DOI

10.1038/s41560-019-0439-6

Peer reviewed

Mn oxidation as the origin of the anomalous capacity of Mn-containing Li-excess cathode materials

Maxwell D. Radin*, Julija Vinckeviciute, Ram Seshadri, Anton Van der Ven*
Materials Department
University of California Santa Barbara, Santa Barbara 93106-5050
*email: maxradin@engineering.ucsb.edu, avdv@engineering.ucsb.edu

Abstract: The Li-excess manganese oxides are a candidate cathode material for the next generation of Li-ion batteries because of their ability to reversibly intercalate more Li than traditional cathode materials. While reversible oxidation of lattice oxygen has been proposed as being at the origin of this excess, anomalous capacity, questions about the underlying electrochemical reaction mechanisms remain unresolved. Here we critically analyze the oxygen redox hypothesis and explore alternative explanations for the origin of the anomalous capacity of Li-excess manganese oxides, including the formation of peroxide ions or trapped oxygen molecules and the oxidation of Mn. First-principles calculations motivated by the Li-Mn-O phase diagram show that the electrochemical behavior of the Li-excess manganese oxides is thermodynamically consistent with the oxidation of Mn from the +4 oxidation state to the +7 oxidation state and the concomitant migration of Mn from octahedral sites to tetrahedral sites. It is shown that the Mn oxidation hypothesis is capable of explaining poorly understood electrochemical behavior of Li-excess materials, including the activation step, the voltage hysteresis, and voltage fade.

Introduction

Li-excess layered manganese oxides[1,2] have attracted widespread attention because of their large reversible capacity, which significantly exceeds that of conventional Li-ion cathode materials.[3–5] Li-excess materials are not only of commercial interest, but also raise fundamental scientific questions because their large reversible capacities cannot be explained by the conventional understanding of redox mechanisms in intercalation compounds. Conventional theories are also unable to explain other unusual electrochemical behavior including: a 4.5 V "activation" plateau during the first charge; a ~0.5 V hysteresis that persists even at low rates;[1,6] and a gradual decrease in the average voltage upon cycling ("voltage fade").[7,8] These features are rarely seen in other intercalation compounds, but appear almost universally across a wide range of layered Li-excess manganese oxides that includes layered Li_2MnO_3[9–11] and its alloys.[1,2,12] Similar behavior is also seen in related compounds such as Mn-containing disordered rocksalts,[13,14] Na-intercalated manganese oxides,[15–18] and some 4d and 5d transition-metal oxides.[19–24]

The most widely accepted interpretation of the anomalous capacity of Li-excess Mn oxides is reversible O^{2-}/O^{-} redox.[25–29] According to this hypothesis, the removal of Li results in the depletion of

non-bonding oxygen p states, resulting in the oxidation of O^{2-} ions to O^{-}. The experimental basis for this interpretation is the absence of evidence for transition metal oxidation[14,26,28,30–34] and the appearance of a localized spectroscopic feature in the oxygen K-edge, which has been attributed to an O^{-} species.[26,30,31,34]

Despite the extensive study of Li-excess materials and the broad acceptance of the oxygen redox hypothesis, a detailed picture of how oxygen redox would lead to an activation plateau, hysteresis, and voltage fade remains elusive. The migration of transition-metal ions to octahedral sites in the Li layer is widely understood to be involved in these phenomena.[7,35,36] It has been suggested that the coupling of oxygen redox to such transition-metal migration could explain the unusual electrochemical behavior of Li-excess materials.[30,37] Nevertheless, while the electrochemical behavior of conventional intercalation electrodes such as Li_xCoO_2 and Li_xFePO_4 can be described with rigorous thermodynamic and kinetic models,[5,38] such models remain largely phenomenological for the Li-excess Mn oxides.[39] Furthermore, the spectroscopic feature attributed to O^{-} is consistent with molecular oxygen and peroxide ions.[31,40–42] These considerations motivate a re-examination of possible redox mechanisms in the Li-excess Mn oxides.

Here we critically analyze the experimental evidence for oxygen redox in Li-excess materials and show that other phenomena, such as the decomposition of the cathode material, can explain the observed spectroscopic features. We then explore alternative mechanisms, including the formation of peroxide ions or trapped oxygen molecules, and the oxidation of Mn^{4+} to Mn^{7+} with concomitant migration from octahedral to tetrahedral sites. While a case for the reversible formation of molecular oxygen or peroxide ions has already been made,[43–45] we argue that Mn^{4+}/Mn^{7+} redox (possibly in concert with the formation of peroxide ions or trapped oxygen molecules) should also be given serious consideration as it is consistent with available experimental evidence and is capable of explaining the activation plateau, voltage hysteresis, and voltage fade. We conclude by noting that there is insufficient experimental evidence to determine to what extent O^{2-}/O^{-} redox and each of the alternative mechanisms occurs and that the fragility of cathode materials at high states of charge may be a major impediment to resolving how much each mechanism contributes to the anomalous capacity.

Critical analysis of oxygen redox

Although “oxygen redox” in principle can refer to any redox process involving oxygen, the anomalous capacity of Li-excess Mn oxides is generally attributed to a specific oxygen redox mechanism: the reversible oxidation of lattice O^{2-} ions to O^{-} ions.[25,26,29] The removal of electrons from oxygen p states, rather than transition-metal d states, has been attributed to a specific local environment: oxygen p states for which neither of the cation sites that it points at are occupied by a transition metal ion.[25] It is important to acknowledge that transition-metal oxides exhibit a high degree of covalency and attributing redox to one particular species is a simplification. For example, prior calculations show that the charge density around oxygen ions changes significantly during the deintercalation of $LiCoO_2$, despite the fact that this reaction nominally operates on the Co^{3+}/Co^{4+} redox couple.[46,47] Despite the subtleties arising from hybridization, formal oxidation states are a powerful tool in understanding intercalation chemistry. In particular, first-principles calculations show that the changes in electronic structure arising from the removal of Li from Li_2MnO_3 and other Mn^{4+} oxides (assuming no other structural rearrangement) can sensibly be interpreted as the reduction of O^{2-} to O^{-}.[25,44] (We emphasize that the O^{2-}/O^{-} oxygen redox mechanism is distinct from the oxygen redox mechanism suggested to

occur during the delithiation of 4d and 5d transition-metal oxides, involving "peroxo-like" $(O_2)^{n-}$ species.[19,22–24])

Although the O^{2-}/O^{-} oxygen redox interpretation has been widely embraced as explaining the anomalous capacity of Li-excess manganese oxides,[24,30,48–50] it represents a radical departure from the corpus of materials chemistry. Localized oxygen holes have been observed as radiation-induced point defects,[51,52] but the notion of a material in which a macroscopic portion of oxygen sites can be interpreted as O^{-} ions is, to our knowledge, unprecedented. (Superconducting cuprates and rare-earth nickelates have been cited as a precedent,[24,53] but these compounds are characterized by a high degree of covalency and generally are not construed to contain an O^{-} species.[54,55]) Being an extraordinary claim, the oxygen redox interpretation of Li-excess manganese oxides requires extraordinary evidence.

The crux of the evidence for the oxygen redox hypothesis is the spectroscopic observation of localized, unoccupied oxygen p states. X-ray absorption spectroscopy shows the appearance of an absorption peak at 531 eV during the first-charge plateau of many different Li-excess manganese oxides.[26,30,31,34,56] Excitation near this energy yields emission at 523 eV.[26,31,56] That the emission at 523 eV is driven by absorption at 531 eV is especially evident in RIXS maps,[30,31,57] demonstrating that these two features are localized to the same species. Similar absorption and emission features are also seen in Na manganese oxides that exhibit an anomalous capacity.[16,17,58]

While the appearance of localized spectroscopic features has been interpreted as the signature of O^{2-}/O^{-} redox, as noted by Xu et al.[31], it is also consistent with the formation of molecular O_2.[41] Similar spectroscopic features have been observed in lithium peroxide.[40,59] In contrast, simulated spectra of stretched peroxide molecules suggest that an O^{-} species would not have an absorption feature near 531 eV.[30] Although it has been suggested that molecular oxygen or peroxide ions are forming reversibly during electrochemical cycling,[34,43–45] such species could also be the product of the irreversible decomposition of the cathode. This would not be surprising given that the release of oxygen gas is typically favored thermodynamically for oxide cathode materials at high states of charge.[5,60] Decomposition could, for example, occur spontaneously after the charged cathode is removed from the electrochemical cell for ex-situ characterization. (To the best of our knowledge, all oxygen K-edge measurements on Li-excess manganese oxides were performed ex situ.) Decomposition could also be triggered by beam damage during spectroscopic experiments. That the changes in the oxygen spectrum are consistent with the formation of molecular O_2 or peroxide ions means that, despite widespread acceptance, there is no direct evidence that compellingly supports the O^{2-}/O^{-} oxygen redox mechanism in the context of Li-excess manganese oxides. Although the absence of direct evidence does not disprove the oxygen redox hypothesis, it motivates a critical re-examination of alternative reaction mechanisms.

Exploration of alternative redox mechanisms

Several other mechanisms have previously been hypothesized to account for the anomalous capacity of the Li-excess Mn oxides, including the release and subsequent reduction of O_2,[61] the formation of oxygen vacancies that enable $Mn^{2+}/Mn^{3+}/Mn^{4+}$ redox,[62–65] the insertion of protons,[10,66] the reversible formation of peroxide ions,[34,43–45] and the oxidation of Mn beyond the +4 oxidation state.[9,67] In this analysis, we reconsider possible mechanisms starting from basic thermodynamic considerations.

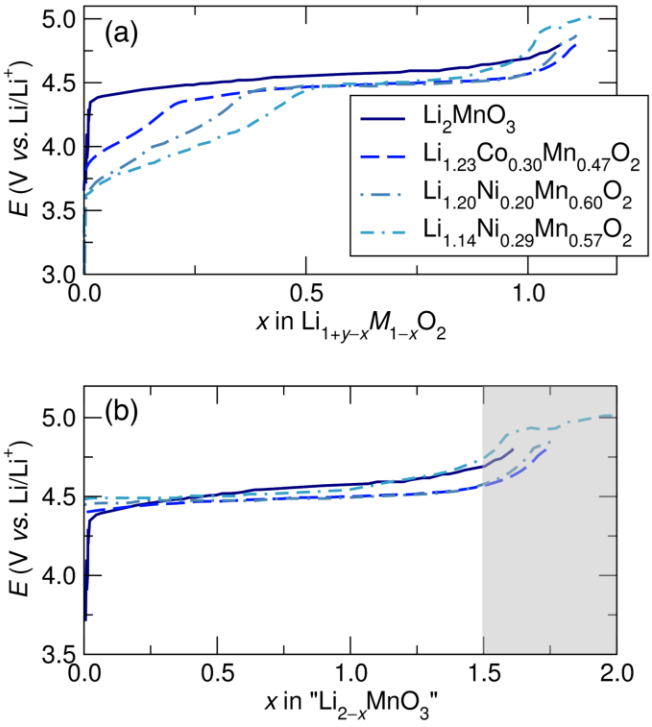

Figure 1. Comparison of the first-charge voltage curves of pure Li_2MnO_3 and Li_2MnO_3/$LiMO_2$ composites. a, the first-charge voltage curves for Li_2MnO_3/$LiMO_2$ composites. b, the portion of the first-charge voltage curves arising from the Li_2MnO_3 component of Li_2MnO_3/$LiMO_2$ composites. The shaded region in (b) highlights that the plateau ends when approximately 1.5 Li have been removed. Data for $Li_{1.20}Ni_{0.20}Mn_{0.60}O_2$, and $Li_{1.14}Ni_{0.29}Mn_{0.57}O_2$ from Ref. [67]; data for $Li_{1.23}Co_{0.30}Mn_{0.47}O_2$ and Li_2MnO_3 from Refs. 6 *and* 11.

The first charge cycle, characterized by a 4.5 V plateau, provides a starting point for analyzing possible redox mechanisms. Figure 1a shows the plateau during the first charge of various Li_2MnO_3–Li*M*O_2 composites[6,67] and pure Li_2MnO_3.[11] (While it is still under debate as to whether such compounds are better described as a solid solution or a coherent two-phase mixture, we will refer to them as composites.) The sloping part of the voltage curves for the composite materials arises from the delithiation of the Li*M*O_2 component, while the plateau is associated with the Li_2MnO_3 component. The universality of the 4.5 V plateau is especially apparent in Figure 1b, which compares the activation plateau of pure Li_2MnO_3 to that of the Li_2MnO_3 component of each Li_2MnO_3–Li*M*O_2 composite, obtained by removing the portion of the voltage curve that corresponds to the theoretical capacity of the Li*M*O_2 component and rescaling the composition axis.

Phase diagrams provide a starting point for understanding the reaction mechanisms that could occur during the activation plateau. The equilibrium pathway resides in the Li–*M*–Mn–O composition space. However, we can restrict ourselves to the Li–Mn–O phase diagram since the voltage and capacity of the activation plateau (relative to the fraction of "Li_2MnO_3") is unaffected by the identity of the other transition metals *M* of the composite (Figure 1)**,** indicating that the activation plateau only involves the Li_2MnO_3 component. The relevant portion of the equilibrium Li–Mn–O phase diagram (as calculated by the Materials Project[68–70]) is shown in Figure 2a. The equilibrium delithiation mechanism, represented by a dashed line, leads to the release of oxygen gas through the reactions

(1) $$Li_2MnO_3 \rightarrow \tfrac{1}{5}Li_4Mn_5O_{12} + \tfrac{3}{10}O_2 + \tfrac{6}{5}Li^+ + \tfrac{6}{5}e^-$$ 3.72 V

and

(2) $$Li_4Mn_5O_{12} \rightarrow 5MnO_2 + O_2 + 4Li^+ + 4e^-.$$ 4.02 V

(Voltages are referenced to Li/Li$^+$ and are computed from data in the Materials Project.[68–70]) Although such a "densification" mechanism was initially thought to be responsible for the first-charge plateau,[1,35,36] this pathway now seems unlikely because the amount of gas detected by differential electrochemical mass spectrometry (DEMS) during the first charge of Li_2MnO_3-LiMO_2 composites is far too small to account for the observed capacity.[26,31,71]

The DEMS measurements cannot rule out the possibility that O_2 could remain trapped within the active material as isolated molecules[44] or small pockets of gas. If such trapped oxygen were reversibly reduced and oxidized on subsequent cycles, the cell would function as a "hybrid Li-ion/Li-O_2" battery.[72] Alternatively, oxygen could be reversibly oxidized to form peroxide dimers. Early ex-situ Raman[26,73] studies failed to detect peroxide ions or molecular oxygen, but recent in-situ studies have observed a Raman peak consistent with peroxide ions.[45] First-principles calculations also suggest that peroxide ions or trapped oxygen molecules could potentially form reversibly in Li-excess materials.[43,44]

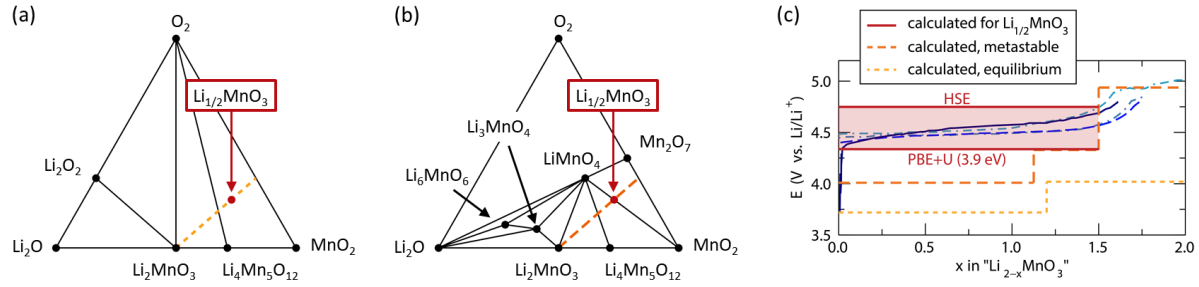

Figure 2. Theoretical phase diagrams and voltage curves for the Li_2O-MnO_2-O_2 system. a, the equilibrium Li_2O-MnO_2-O_2 phase diagram shows that the equilibrium delithiation mechanism (represented by the dashed line) involves the evolution of O_2 gas. b, the metastable phase diagram shows that if the formation of oxygen-oxygen bonds were kinetically impeded, then delithiation could occur via the oxidation of Mn to the +7 oxidation state in the form of $LiMnO_4$ and Mn_2O_7. In both (a) and (b), the hypothesized $Li_{1/2}MnO_3$ phase, which is not a ground state in either phase diagram, is represented by a red dot. c, comparison between the experimental voltage curves for Li_2MnO_3 and the Li_2MnO_3 component of composites,[6,11,67] and the theoretical voltage curves for three mechanisms: the equilibrium pathway on the phase diagram in panel (a), the equilibrium pathway on the metastable phase diagram shown in panel (b), and the delithiation of Li_2MnO_3 to $Li_{1/2}MnO_3$. The experimental voltage curves are the same as those shown in Figure 1b. The spread on predicted voltages for the Li_2MnO_3 to $Li_{1/2}MnO_3$ pathway using different first-principles approaches (i.e. PBE+U and HSE) is shown as a red band.

While the reversible formation of molecular oxygen or peroxide ions has been invoked to explain the behavior of Li-excess materials,[34,43–45] here, we explore an alternative mechanism that has as of yet received little consideration: the oxidation of Mn from a formal oxidation state of +4 to +7. The importance of this mechanism is revealed when we explore a scenario where the dimerization of oxygen is kinetically limited. To this end, we consider the metastable phase diagram obtained by excluding all phases that exhibit covalent oxygen-oxygen bonds (i.e. O_2, Li_2O_2, LiO_2, and LiO_3). Within this metastable phase diagram, the equilibrium reaction pathway (represented by the dashed line in Figure 2b) occurs via the oxidation of Mn^{4+} to Mn^{7+} through a series of three-phase reactions that yield the Mn^{4+} compounds MnO_2 and $Li_4Mn_5O_{12}$ and the Mn^{7+} compounds $LiMnO_4$ and Mn_2O_7.

The observed voltage curves suggest that the system does not follow this sequence of reactions. Figure 2c compares the experimentally observed first-charge voltage curves for Li_2MnO_3[11] and the

Li_2MnO_3 components of composite materials[6,67] with the calculated voltage curves for the metastable reaction pathway (dashed orange line) and the true equilibrium pathway (dashed yellow line). The absence of a step at $x = 9/8$ in the observed voltage curves implies that the reaction does not proceed by the above three-phase reactions.

It would not be surprising for these three-phase reactions to be kinetically slow, as they require the long-range diffusion of Mn or O. For example, if the oxygen sublattice were to remain intact, Li extraction would need to be accompanied by a redistribution of Mn such that some regions become enriched in Mn and others become depleted. The sluggish mobility of Mn relative to that of Li makes this scenario unlikely, suggesting a kinetically simpler reaction that results in a metastable $Li_{2-x}MnO_3$ compound according to:

(3) $$\mathrm{Li_2MnO_3} \rightarrow \mathrm{Li_{2-x}MnO_3} + x\mathrm{Li^+} + xe^-.$$

The notion of a metastable $Li_{2-x}MnO_3$ phase forming on first charge is not new: the oxygen-redox hypothesis represents the formation of a metastable $Li_{2-x}MnO_3$ phase where some of the oxygen anions are in the −1 oxidation state.[25,29,37] However, the fact that the equilibrium phases (within the metastable phase diagram of Figure 2b) contain Mn^{4+} and Mn^{7+} suggests that the $Li_{2-x}MnO_3$ reaction product could be a mixed-valence Mn^{4+}/Mn^{7+} compound. This is further motivated by the fact that many of the Mn^{4+} and Mn^{7+} phases in the metastable phase diagram favor fcc oxygen sublattices[74–77] and therefore could form a solid solution or nanocomposite.

Critical analysis of Mn oxidation

To explore the possible formation of $Li_{2-x}MnO_3$ compounds containing Mn^{4+} and Mn^{7+}, we calculated the energies of $Li_{1/2}MnO_3$ structures that have an fcc oxygen sublattice from first principles. This composition (represented by a red circle in Figure 2a and Figure 2b) approximates the capacity at the end of the first-charge plateau and requires the oxidation of one half of the Mn^{4+} ions to Mn^{7+}. Because Mn^{4+} prefers octahedral coordination[74] and Mn^{7+} prefers tetrahedral coordination,[76] we considered structures wherein half of the Mn reside in tetrahedral sites and half in octahedral sites. The lowest energy structure found is shown in Figure 3a. (See Supporting Information for additional details.)

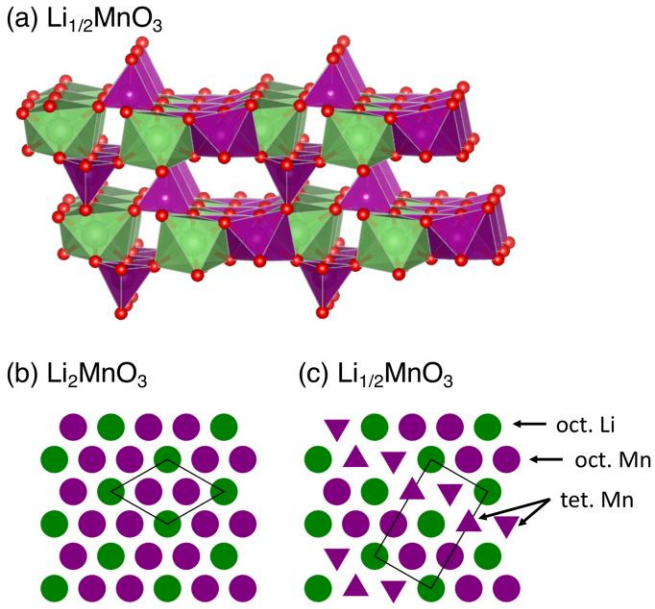

Figure 3. Hypothesized $Li_{1/2}MnO_3$ structure representing the Li_2MnO_3 component of the cathode material at the end of the activation plateau. a, Relaxed crystal structure for the hypothesized $Li_{1/2}MnO_3$ structure, with green, purple, and red corresponding to Li, Mn, and O. b and c, Comparison of the Li_2MnO_3 and hypothesized $Li_{1/2}MnO_3$ structures. The circles represent the octahedral sites within the transition-metal layer. The triangles represent the tetrahedral sites in the Li layer that reside directly above and below the octahedral sites in the transition-metal layer. The black lines denote the unit cell.

The voltage for the reaction $\mathrm{Li_2MnO_3 \rightarrow Li_{½}MnO_3 + ¾Li^+ + ¾e^-}$ calculated with DFT+*U*, *U* = 3.9 eV is 4.34 V (the predicted voltage is 4.55 V when *U* = 5 eV). The hybrid functional HSE predicts a slightly higher voltage of 4.75 V. These values are consistent with the experimentally observed voltage considering that the error in intercalation voltages for transition-metal oxides predicted by DFT+*U* and HSE is often several tenths of a volt.[78] Preliminary calculations (using PBE+*U*, HSE, and SCAN functionals, see Supplementary Information) also suggest that Mn oxidation is thermodynamically favored over lattice oxygen redox. However, as discussed in Supplementary Information, a definitive determination of which mechanism is thermodynamically favored will require more advanced approaches to electronic structure calculations.

The energy for a phase to decompose into its equilibrium state can serve as a rough guide as to whether that phase can be produced in a laboratory.[79] The energy for the decomposition of $Li_{1/2}MnO_3$ into the metastable phases of Figure 2b through the reaction $\mathrm{Li_{½}MnO_3 \rightarrow ½LiMnO_4 + ½MnO_2}$ is −0.15 eV/atom. Further decomposition into the true equilibrium state through the reaction

(3) $$\mathrm{½LiMnO_4 + ½MnO_2 \rightarrow ⅛Li_4Mn_5O_{12} + ⅜MnO_2 + ⅜O_2}$$

has an energy of −0.10 eV/atom. (Including the entropy of gas-phase O_2 under standard conditions[80] yields a reaction free energy of −0.15 eV/atom.) Given that these reaction energies are comparable to the decomposition energies of other metastable compounds that can be synthesized under laboratory conditions,[79] it is plausible that $Li_{1/2}MnO_4$ could form during an electrochemical experiment.

The hypothesized $Li_{1/2}MnO_3$ structure is intended to be a representative model of the local structure of the charged Li_2MnO_3 component of Li-excess manganese oxides, and other $Li_{2-x}MnO_3$ configurations

with similar local structure could also form upon charge before $Li_{1/2}MnO_3$. The presence of a non-negligible slope in the 4.5 V "plateau" of Figure 1b could be due to the formation of such configurations. A key property of the $Li_{1/2}MnO_3$ structure shown in Figure 3a is that it provides each oxygen site with a local environment that is consistent with Pauling's second rule.[81] Structures with severe violations of Pauling's second rule were predicted to be significantly higher in energy.

Mixed-valence Mn^{4+}/Mn^{7+} phases similar to that of Figure 3a are kinetically accessible from the original Li_2MnO_3 phase because their formation only requires a single octahedral to tetrahedral hop for each Mn that migrates. Figure 3b and c illustrate how Li_2MnO_3 could topotactically transform into $Li_{1/2}MnO_3$. Two-thirds (one-third) of the octahedral sites of the transition-metal layer of Li_2MnO_3 are occupied by Mn (Li), as shown in Figure 3b. Figure 3c shows how the hypothesized $Li_{1/2}MnO_3$ structure can emerge if one quarter of the Mn atoms migrate to tetrahedral sites in the lithium layer above (upwards-pointing triangles) and one quarter of the Mn atoms migrate to tetrahedral sites in the lithium layer below (downward-pointing triangles).

If discharge proceeds via the reduction of Mn^{7+} to Mn^{4+}, then the availability of multiple tetrahedral→octahedral migration pathways can explain the absence of the 4.5 V plateau on subsequent cycles: tetrahedral Mn ions are unlikely to return to their original octahedral sites during the first discharge. A tetrahedral Mn ion can migrate to any of the four octahedral sites with which it shares a face. (In the $Li_{1/2}MnO_3$ structure of Figure 3a, one of these sites is likely inaccessible because it shares a face with another tetrahedral Mn ion.) After the first discharge, the cation ordering (within the Li_2MnO_3 component) is likely to resemble a disordered rocksalt more than layered Li_2MnO_3. The second-charge voltage curve will then differ from the first-charge voltage curve, with the diversity of local Mn environments yielding contributions to the capacity across a wide voltage range. Voltage fade upon further cycling[7] could arise from further rearrangement of Mn ions.

The migration of Mn between tetrahedral and octahedral sites can also explain the large hysteresis in the voltage curve.[6,82,83] If the kinetics of Mn migration between octahedral and tetrahedral sites is rate limiting, then discharge could proceed via the reduction of Mn^{7+} to Mn^{5+}, which would not require the migration of manganese ions because Mn^{5+} favors tetrahedral coordination.[84] The difference in voltage between the Mn^{4+}/Mn^{7+} and Mn^{5+}/Mn^{7+} redox couples would manifest as a polarization in the voltage curve, and energy would be lost in the form of heat released by the gradual migration of manganese ions to octahedral sites. (The reduction of octahedral Mn^{4+} remaining at the end of charge to Mn^{3+} could similarly occur without manganese migration.) Such a process is analogous to how sluggish diffusion can lead to hysteresis in conversion electrodes.[83]

The notion that octahedral/tetrahedral migration is responsible for the unusual electrochemical behavior of the Li-excess manganese oxides is supported by similar behavior in $LiCrO_2 \cdot Li_2MnO_3$ composites. In these materials, (de)intercalation below 4.4 V operates on the Cr^{3+}/Cr^{6+} redox couple and is accompanied by the migration of Cr between octahedral and tetrahedral sites.[85–87] The voltage profile of these composites changes dramatically after the first charge, and this "activation" phenomenon has been attributed to the migration of Cr ions to octahedral sites in the Li layer during the first discharge.[87] During subsequent cycling, $LiCrO_2 \cdot Li_2MnO_3$ composites also exhibit a significant polarization (~0.3 V).[85] A similar activation and hysteresis have also been observed in $LiCrO_2 \cdot Li_2TiO_3$ composites.[88]

If reversible Mn^{4+}/Mn^{7+} redox were responsible for the anomalous capacity of Li-excess Mn oxides, then experimental verification would be challenging because of the fragility of oxides containing Mn^{7+}.

For example, beam damage can reduce Mn^{7+} to Mn^{4+} in $KMnO_4$ during Mn K- and L-edge X-ray absorption experiments,[89,90] as well as in Mn L-edge electron energy-loss spectroscopy.[91] Experiments have also found $KMnO_4$ to decompose during O K-edge X-ray absorption measurements.[92] (Although studies on Mn^{7+} compounds such as $KMnO_4$ can provide a useful guide as to the fragility of a Mn^{7+}-containing cathode, a charged Li-excess cathode could potentially be degraded more rapidly than reference compounds due to differences in bonding, particle size, and microstructure.) The spectroscopic observation of Mn^{4+} in charged cathodes therefore does not definitively rule out the presence of Mn^{7+}. Experiments showing that beam damage can induce a RIXS feature in $LiAlO_2$ that is identical to the feature observed in charged Li-excess cathodes[42] support this scenario, as does the observation of a similar RIXS feature in Li_2O.[40] Lastly, we note that in-situ beam damage may not significant affect electrochemical performance because in typical experiments, the beam covers only a small fraction of the electrode area.

Despite the fragility of Mn^{7+} compounds, there is experimental evidence to suggest the presence of Mn^{7+} at the end of charge. First, although the smallness of the pre-edge peak indicates that most of the signal originates from octahedral Mn, changes in the Mn K edge measured in situ are consistent with the formation of a small amount of Mn^{7+}. These changes include a shift of the main peak to higher energy and a growth of the pre-edge peak.[11,26,28,30] Second, a recent in-situ diffraction study on a Li-excess cathode concluded that transition-metal ions migrate to tetrahedral sites in the Li layer during charge and return to octahedral sites on discharge.[93] Lastly, the Raman feature attributed to the reversible formation of peroxide ions is also consistent with tetrahedral Mn^{7+}.[45,94]

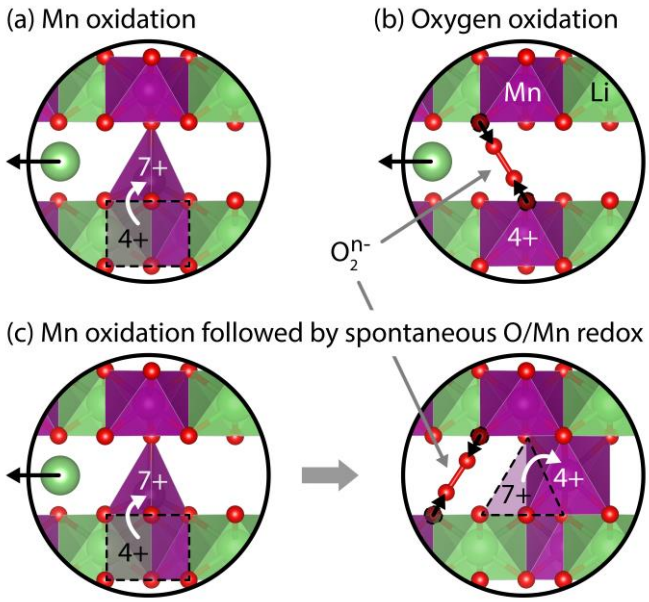

Figure 4. Alternative charge mechanisms in Li-excess Mn oxides. a, the oxidation of Mn^{4+} to Mn^{7+}. b, the oxidation of oxygen ions to form peroxide ions or internally trapped oxygen molecules. c, the oxidation of Mn^{4+} to Mn^{7+} followed by the spontaneous formation of peroxide ions or trapped oxygen molecules and the reduction of Mn.

Figure 4(a) and (b) illustrates the two alternatives to the lattice oxygen redox hypothesis that we have explored so far. While the formation of Mn^{7+} (**Error! Reference source not found.**a) as a charge mechanism is quite distinct to the formation of internally trapped O_2 molecules or peroxide ions (**Error! Reference source not found.**b), the two mechanisms could be linked. The migration of Mn to

tetrahedral sites could trigger the spontaneous formation of O_2 molecules or peroxide ions, in which case the Mn^{7+} ions would be reduced and likely return to octahedral sites, as shown in **Error! Reference source not found.**c. This scenario is consistent with spectroscopic observations showing Mn mainly in the +4 oxidation stateand also can explain the activation process and hysteresis. The disappearance of the activation plateau after the first cycle could arise from the availability of multiple tetrahedral→octahedral migration pathways as discussed above, and the spontaneous formation of oxygen dimers could lead to hysteresis because charge and discharge would follow different reaction pathways: while charge would occur via the oxidation of Mn^{4+} to Mn^{7+}, discharge would occur via the reduction of O_2 or O_2^{2-} to O^{2-}.

In the case of pure Li_2MnO_3, the observation of significant O_2 release through DEMS during the first charge and poor electrochemical reversibility[11] are consistent with the spontaneous decomposition of a Mn^{7+} phase. Other kinetic processes leading to oxygen evolution, such as the densification mechanism discussed above, may also occur. However, the agreement between the first-charge voltage curves (when appropriately normalized) of Li_2MnO_3 and composite materials suggests that the electrochemical process occurring in these compounds is the same. Therefore the embedding of Li_2MnO_3 in a nanocomposite may play an important role in stabilizing the Mn^{7+} phase formed on charge or stabilizing a structure containing peroxide ions or trapped oxygen molecules.

Conclusion

The experimental evidence for O^{2-}/O^{-} lattice oxygen redox in Li-excess materials is not yet conclusive and alternative mechanisms require renewed attention. (We emphasize that although available experimental observations do not provide compelling direct evidence for O^{2-}/O^{-} redox, they also do not definitively rule it out.) We have highlighted several mechanisms that appear to be consistent with available data (illustrated in Figure 4): the oxidation of Mn^{4+} to Mn^{7+} accompanied by a migration from octahedral to tetrahedral sites; the formation of peroxide ions or trapped molecular oxygen; and the formation of Mn^{7+} followed by the spontaneous dimerization of oxygen. We have explored in depth the oxidation of Mn^{4+} to Mn^{7+} and found this hypothesis to be compatible with experimental and first-principles thermodynamics, supported by the observation of tetrahedral occupancy at the end of charge through XRD,[93] and consistent with the electrochemical behavior in Cr-based cathode materials which are known to undergo tetrahedral/octahedral migration.[85–88] The anomalous capacity may, however, involve contributions from multiple redox mechanisms. Furthermore, the redox mechanism on charge may be different from that on discharge (e.g., the oxidation of Mn on charge and reduction of or peroxide ions or trapped oxygen molecules on discharge). Advances in both experimental and theoretical methods could lead to a clearer understanding of the roles that different mechanisms play. New innovations in in-situ experimental probes may be especially valuable because the excess capacity originates at high states of charge, where almost all intercalation compounds are metastable and highly susceptible to decomposition reactions. Techniques to probe for peroxide ions or molecular oxygen deep within cathode particles could also provide great insight.

Although our analysis focused on the Li-excess manganese oxides, the mechanisms discussed above could explain the anomalous capacity of certain manganese oxides used as electrodes in Na-ion batteries.[15–18,95] These materials behave similarly to the Li-excess manganese oxides in that they exhibit an anomalous capacity and significant polarization. However, they differ in that there is no apparent "activation": the charge curve does not qualitatively change after the first cycle. This could arise from

the large size of the Na^+ ions relative to Mn^{4+} ions, which makes it unfavorable for Na^+ and Mn^{4+} ions to reside in the same layer. This scenario is supported by recent experiments on a Zn-doped Na manganese oxide:[18] transmission electron microscopy indicated that cations migrated from the transition-metal layer to the Na layer during charge and returned to the transition-metal layer on discharge.

These mechanisms could also explain the behavior of certain 4d/5d transition-metal oxides.[19–24] The electrochemical activity of these materials has been attributed to a combination of the oxidation of octahedral Ir/Ru ions and oxygen redox involving the formation of a peroxo-like $(O_2)^{n-}$ species or a true peroxide O_2^{2-}.[20,23,24,31,53,96,97] The electrochemical behavior of these materials is nevertheless also consistent with the migration of oxidized Ir and Ru ions between octahedral and tetrahedral sites, as discussed in the Supporting Information. A RIXS feature similar to that observed in Li-excess Mn oxides has also been observed in charged $Li_2Ir_{1/2}Sn_{1/2}O_3$, and could represent the decomposition products of a compound containing highly oxidized Ir.[20] Additionally, Raman signals associated with the anomalous capacity of Na_3RuO_4 and attributed to peroxide ions are also consistent with tetrahedral Ru^{7+}.[97,98]

If the Mn-oxidation mechanism is correct, it suggests a guiding principle for the design of high-capacity cathode materials: the use of a nanocomposite or alloy may allow one to access high oxidation states that otherwise would lead to the decomposition of the material. A challenge of such an approach is to manage the migration of transition-metal ions, as large changes in oxidation state are often accompanied by a change in coordination preferences. It may be possible to design cathode materials that utilize high oxidation states without inducing transition-metal migration or to design materials where the migration of transition-metal ions is sufficiently facile and reversible to yield satisfactory electrochemical performance.

Computational Methods

DFT calculations were performed with the Vienna ab initio Simulation Package (VASP)[99–102] with projector augmented-wave (PAW) pseudopotentials.[103] All calculations were spin polarized, employed plane-wave basis sets with 530 eV energy cutoffs. PBE+*U*[104] calculations on oxides sampled the Brillouin zone with a k-point mesh density of at least 26 Å, while HSE[105,106] calculations on oxides used a coarser density of at least 10 Å. Calculations on the primitive cell of bcc Li used a denser k-point mesh of 10 × 10 × 10. The PBE+*U* calculations employed the on-site Coulomb correction of Dudarev et al.[107] for Mn d states with U_{eff} = 3.9 eV and 5 eV. HSE calculations used the standard mixing parameter α of 0.25. Relaxations used Gaussian smearing of width 0.2 eV and were converged to within a force convergence criterion of 0.02 eV/Å for both PBE+*U* and HSE calculations; these were followed by single-point calculations using the tetrahedron method with Blöchl corrections[108] in order to obtain accurate energies. Because magnetic studies show that interactions between edge-sharing Mn^{4+} ions are ferromagnetic,[109] our calculations were restricted to ferromagnetic spin orderings.

Data Availability Statement

The authors affirm that the analysis presented here can be reproduced with the data provided in the paper, supporting information, and cited references. Additional calculation data generated during this study are available upon reasonable request.

Acknowledgements

We thank L. Piper and Z. Lebens-Higgins for valuable discussion. This work was supported as part of the NorthEast Center for Chemical Energy Storage (NECCES), an Energy Frontier Research Center funded by the U.S. Department of Energy, Office of Science, Basic Energy Sciences under Award # DE-SC0012583. The contributions of RS were supported as part of the Center for Synthetic Control Across Length-scales for Advancing Rechargeables (SCALAR), an Energy Frontier Research Center funded by the U.S. Department of Energy, Office of Science, Basic Energy Sciences under Award # DE-SC0019381. This research used resources of the National Energy Research Scientific Computing Center (NERSC), a U.S. Department of Energy Office of Science User Facility operated under Contract No. DE-AC02-05CH11231. Use of the Center for Scientific Computing at UC Santa Barbara supported by the National Science Foundation (NSF) Materials Research Science and Engineering Centers program through NSF DMR 1720256, and NSF CNS 1725797 is also acknowledged.

References

1. Lu, Z., Beaulieu, L. Y., Donaberger, R. A., Thomas, C. L. & Dahn, J. R. Synthesis, Structure, and Electrochemical Behavior of $Li[Ni_xLi_{1/3-2x/3}Mn_{2/3-x/3}]O_2$. *J. Electrochem. Soc.* **149**, A778 (2002).

2. Johnson, C. S. *et al.* The significance of the Li_2MnO_3 component in 'composite' $xLi_2MnO_3{\cdot}(1-x)LiMn_{0.5}Ni_{0.5}O_2$ electrodes. *Electrochem. commun.* **6**, 1085–1091 (2004).

3. Hong, J., Gwon, H., Jung, S.-K., Ku, K. & Kang, K. Review—Lithium-Excess Layered Cathodes for Lithium Rechargeable Batteries. *J. Electrochem. Soc.* **162**, A2447–A2467 (2015).

4. Hy, S. *et al.* Performance and Design Considerations For The lithium Excess Layered Oxide Positive Electrode Materials For Lithium Ion Batteries. *Energy Environ. Sci.* **9**, 1931–1954 (2016).

5. Radin, M. D. *et al.* Narrowing the Gap Between Theoretical and Practical Capacities in Li-ion Layered Oxide Cathode Materials. *Adv. Energy Mater.* 1602888 (2017). doi:10.1002/aenm.201602888

6. Wei, Y. J. *et al.* Electrochemical kinetics and cycling performance of nano $Li[Li_{0.23}Co_{0.3}Mn_{0.47}]O_2$ cathode material for lithium ion batteries. *Electrochem. commun.* **11**, 2008–2011 (2009).

7. Johnson, C. S., Li, N., Lefief, C., Vaughey, J. T. & Thackeray, M. M. Synthesis , Characterization and Electrochemistry of Lithium Battery Electrodes: $xLi_2MnO_3{\cdot}(1-x)LiMn_{0.333}Ni_{0.333}Co_{0.333}O_2$ ($0 \le x \le 0.7$). *Chem. Mater.* **20**, 6095–6106 (2008).

8. Bettge, M. *et al.* Voltage Fade of Layered Oxides: Its Measurement and Impact on Energy Density. *J. Electrochem. Soc.* **160**, A2046–A2055 (2013).

9. Kalyani, P., Chitra, S., Mohan, T. & Gopukumar, S. Lithium metal rechargeable cells using Li_2MnO_3 as the positive electrode. *J. Power Sources* **80**, 103–106 (1999).

10. Robertson, A. D. & Bruce, P. G. Mechanism of Electrochemical Activity in Li_2MnO_3. *Chem. Mater.* **15**, 1984–1992 (2003).

11. Yu, D. Y. W., Yanagida, K., Kato, Y. & Nakamura, H. Electrochemical Activities in Li_2MnO_3. *J. Electrochem. Soc.* **156**, A417 (2009).

12. Park, Y. J. *et al.* Synthesis and Electrochemical Characteristics of $Li[Co_xLi_{(1/3-x/3)}Mn_{(2/3-2x/3)}]O_2$

Compounds. *J. Electrochem. Soc.* **151**, A720 (2004).

13. Yabuuchi, N. *et al.* High-capacity Electrode Materials for Rechargeable Lithium Batteries: Li_3NbO_4-Based System with Cation-Disordered Rocksalt Structure. *Proc. Natl. Acad. Sci. U. S. A.* **112**, 7650–7655 (2015).

14. Yabuuchi, N. *et al.* Origin of stabilization and destabilization in solid-state redox reaction of oxide ions for lithium-ion batteries. *Nat. Commun.* **7**, 13814 (2016).

15. Yabuuchi, N. *et al.* A new electrode material for rechargeable sodium batteries: P2-type $Na_{2/3}[Mg_{0.28}Mn_{0.72}]O_2$ with anomalously high reversible capacity. *J. Mater. Chem. A* **2**, 16851–16855 (2014).

16. Maitra, U. *et al.* Oxygen redox chemistry without excess alkali-metal ions in $Na_{2/3}[Mg_{0.28}Mn_{0.72}]O_2$. *Nat. Chem.* **10**, 288–295 (2018).

17. Mortemard de Boisse, B. *et al.* Highly Reversible Oxygen-Redox Chemistry at 4.1 V in $Na_{4/7-x}[\square_{1/7}Mn_{6/7}]O_2$ (□: Mn Vacancy). *Adv. Energy Mater.* **2**, 1800409 (2018).

18. Bai, X. *et al.* Anionic Redox Activity in a Newly Zn-Doped Sodium Layered Oxide P2-$Na_{2/3}Mn_{1-y}Zn_yO_2$ ($0 < y < 0.23$). *Adv. Energy Mater.* **8**, 1802379 (2018).

19. Sathiya, M. *et al.* Reversible anionic redox chemistry in high-capacity layered-oxide electrodes. *Nat. Mater.* **12**, 827–35 (2013).

20. Hong, J. *et al.* Metal–oxygen decoordination stabilizes anion redox in Li-rich oxides. *Nat. Mater.* doi:10.1038/s41563-018-0276-1

21. Pearce, P. E. *et al.* Evidence for anionic redox activity in a tridimensional-ordered Li-rich positive electrode β-Li_2IrO_3. *Nat. Mater.* **16**, 580–586 (2017).

22. McCalla, E. *et al.* Visualization of O-O peroxo-like dimers in high-capacity layered oxides for Li-ion batteries. *Science* **350**, 1516–21 (2015).

23. Saubanère, M., McCalla, E., Tarascon, J.-M. & Doublet, M.-L. The intriguing question of anionic redox in high-energy density cathodes for Li-ion batteries. *Energy Environ. Sci.* **9**, 984–991 (2016).

24. Assat, G. & Tarascon, J. Fundamental understanding and practical challenges of anionic redox activity in Li-ion batteries. *Nat. Energy* **3**, 373–386 (2018).

25. Seo, D. *et al.* The electronic origin of the oxygen redox activity in Li-excess cathode materials. *Nat. Chem.* **8**, 692–697 (2016).

26. Luo, K. *et al.* Charge-compensation in 3d-transition-metal-oxide intercalation cathodes through the generation of localized electron holes on oxygen. *Nat. Chem.* **8**, 1–17 (2016).

27. Koga, H. *et al.* Different oxygen redox participation for bulk and surface: A possible global explanation for the cycling mechanism of $Li_{1.20}Mn_{0.54}Co_{0.13}Ni_{0.13}O_2$. *J. Power Sources* **236**, 250–258 (2013).

28. Koga, H. *et al.* Operando X-ray Absorption Study of the Redox Processes Involved upon Cycling of the Li-Rich Layered Oxide $Li_{1.20}Mn_{0.54}Co_{0.13}Ni_{0.13}O_2$ in Li Ion Batteries. *J. Phys. Chem. C* **118**, 5700–5709 (2014).

29. Koyama, Y., Tanaka, I., Nagao, M. & Kanno, R. First-principles study on lithium removal from

Li_2MnO_3. *J. Power Sources* **189**, 798–801 (2009).

30. Gent, W. E. *et al.* Coupling between oxygen redox and cation migration explains unusual electrochemistry in lithium-rich layered oxides. *Nat. Commun.* **8**, 2091 (2017).

31. Xu, J. *et al.* Elucidating anionic oxygen activity in lithium-rich layered oxides. *Nat. Commun.* **9**, 947 (2018).

32. Kubobuchi, K. *et al.* Mn $L_{2,3}$-edge X-ray absorption spectroscopic studies on charge-discharge mechanism of Li_2MnO_3. *Appl. Phys. Lett.* **104**, 2–6 (2014).

33. Rana, J. *et al.* Structural Changes in Li_2MnO_3 Cathode Material for Li-Ion Batteries. *Adv. Energy Mater.* **4**, 1300998 (2014).

34. Oishi, M. *et al.* Direct observation of reversible charge compensation by oxygen ion in Li-rich manganese layered oxide positive electrode material, $Li_{1.16}Ni_{0.15}Co_{0.19}Mn_{0.50}O_2$. *J. Power Sources* **276**, 89–94 (2015).

35. Tran, N. *et al.* Mechanisms associated with the 'plateau' observed at high voltage for the overlithiated $Li_{1.12}Ni_{0.425}Mn_{0.425}Co_{0.15})_{0.88}O_2$ system. *Chem. Mater.* **20**, 4815–4825 (2008).

36. Armstrong, A. R. *et al.* Demonstrating oxygen loss and associated structural reorganization in the lithium battery cathode $Li[Ni_{0.2}Li_{0.2}Mn_{0.6}]O_2$. *J. Am. Chem. Soc.* **128**, 8694–8698 (2006).

37. Lee, E. & Persson, K. A. Structural and Chemical Evolution of the Layered Li-Excess Li_xMnO_3 as a Function of Li Content from First-Principles Calculations. *Adv. Energy Mater.* **4**, 1400498 (2014).

38. Malik, R., Abdellahi, A. & Ceder, G. A Critical Review of the Li Insertion Mechanisms in $LiFePO_4$ Electrodes. *J. Electrochem. Soc.* **160**, A3179–A3197 (2013).

39. Rinaldo, S. G. *et al.* Physical Theory of Voltage Fade in Lithium- and Manganese-Rich Transition Metal Oxides. *J. Electrochem. Soc.* **162**, A897–A904 (2015).

40. Zhuo, Z. *et al.* Spectroscopic Signature of Oxidized Oxygen States in Peroxides. *J. Phys. Chem. Lett.* doi:10.1021/acs.jpclett.8b02757 (2018). doi:10.1021/acs.jpclett.8b02757

41. Glans, P. *et al.* Resonant x-ray emission spectroscopy of molecular oxygen. *Phys. Rev. Lett.* **76**, 2448–2451 (1996).

42. Lebens-Higgins, Z. W. *et al.* Distinction Between Intrinsic and X-ray Induced Oxidized Oxygen States in Li-Rich 3d Layered Oxides and $LiAlO_2$. *J. Phys. Chem. C* acs.jpcc.9b01298 (2019). doi:10.1021/acs.jpcc.9b01298

43. Bercx, M., Slap, L., Partoens, B. & Lamoen, D. First-Principles Investigation of the Stability of the Oxygen Framework of Li-Rich Battery Cathodes. *MRS Adv.* **4**, 813–820 (2017).

44. Chen, H. & Islam, M. S. Lithium extraction mechanism in Li-rich Li_2MnO_3 involving oxygen hole formation and dimerization. *Chem. Mater.* **28**, 6656–6663 (2016).

45. Li, X. *et al.* Direct Visualization of the Reversible O_2−/O− Redox Process in Li-Rich Cathode Materials. *Adv. Mater.* **30**, 1705197- (2018).

46. Van der Ven, A., Aydinol, M. K., Ceder, G., Kresse, G. & Hafner, J. First-principles investigation of phase stability in Li_xCoO_2. *Phys. Rev. B* **58**, 2975–2987 (1998).

47. Wolverton, C. & Zunger, A. First-Principles Prediction of Vacancy Order-Disorder and Intercalation Battery Voltages in Li_xCoO_2. *Phys. Rev. Lett.* **81**, 606–609 (1998).

48. Qiu, B., Zhang, M., Xia, Y., Liu, Z. & Meng, Y. S. Understanding and Controlling Anionic Electrochemical Activity in High-Capacity Oxides for Next Generation Li-Ion Batteries. *Chem. Mater.* **29**, 908–915 (2017).

49. Okubo, M. & Yamada, A. Molecular Orbital Principles of Oxygen-Redox Battery Electrodes. *ACS Appl. Mater. Interfaces* **9**, 36463–36472 (2017).

50. Li, B. & Xia, D. Anionic Redox in Rechargeable Lithium Batteries. *Adv. Mater.* **29**, 1–28 (2017).

51. Schirmer, O. F. Smoky coloration of quartz caused by bound small hole polaron optical absorption. *Solid State Commun.* **18**, 1349–1351 (1976).

52. Griscom, D. L. Self-trapped holes in pure-silica glass: A history of their discovery and characterization and an example of their critical significance to industry. *J. Non. Cryst. Solids* **352**, 2601–2617 (2006).

53. Grimaud, A., Hong, W. T., Shao-Horn, Y. & Tarascon, J. M. Anionic redox processes for electrochemical devices. *Nat. Mater.* **15**, 121–126 (2016).

54. Lee, P. A., Nagaosa, N. & Wen, X. G. Doping a Mott insulator: Physics of high-temperature superconductivity. *Rev. Mod. Phys.* **78**, (2006).

55. Subedi, A., Peil, O. E. & Georges, A. Low-energy description of the metal-insulator transition in the rare-earth nickelates. *Phys. Rev. B* **91**, 075128 (2015).

56. Hu, E. *et al.* Evolution of redox couples in Li- and Mn-rich cathode materials and mitigation of voltage fade by reducing oxygen release. *Nat. Energy* **3**, (2018).

57. Yang, W. & Devereaux, T. P. Anionic and cationic redox and interfaces in batteries: Advances from soft X-ray absorption spectroscopy to resonant inelastic scattering. *J. Power Sources* **389**, 188–197 (2018).

58. Dai, K. *et al.* High Reversibility of Lattice Oxygen Redox in Na-ion and Li-ion Batteries Quantified by Direct Bulk Probes of both Anionic and Cationic Redox Reactions. *Joule* doi:10.1016/j.joule.2018.11.014 (2018). doi:10.1016/j.joule.2018.11.014

59. Chan, M. K. Y. *et al.* Structure of Lithium Peroxide. *J. Phys. Chem. Lett.* **2**, 2483–2486 (2011).

60. Wang, L., Maxisch, T. & Ceder, G. A First-Principles Approach to Studying the Thermal Stability of Oxide Cathode Materials. *Chem. Mater.* **19**, 543–552 (2007).

61. Yabuuchi, N., Yoshii, K., Myung, S. T., Nakai, I. & Komaba, S. Detailed studies of a high-capacity electrode material for rechargeable batteries, Li_2MnO_3-$LiCo_{1/3}Ni_{1/3}Mn_{1/3}O_2$. *J. Am. Chem. Soc.* **133**, 4404–4419 (2011).

62. Lu, Z. & Dahn, J. R. Understanding the Anomalous Capacity of Li/$Li[Ni_xLi_{(1/3-2x/3)}Mn_{(2/3-x/3)}]O_2$ Cells Using In Situ X-Ray Diffraction and Electrochemical Studies. *J. Electrochem. Soc.* **149**, A815 (2002).

63. Pasero, D., McLaren, V., De Souza, S. & West, A. R. Oxygen nonstoichiometry in Li_2MnO_3: An alternative explanation for its anomalous electrochemical activity. *Chem. Mater.* **17**, 345–348 (2005).

64. Kubota, K. *et al.* Direct synthesis of oxygen-deficient Li_2MnO_{3-x} for high capacity lithium battery electrodes. *J. Power Sources* **216**, 249–255 (2012).

65. Okamoto, Y. Ambivalent Effect of Oxygen Vacancies on Li_2MnO_3: A First-Principles Study. *J. Electrochem. Soc.* **159**, A152–A157 (2012).

66. Armstrong, A. R., Robertson, A. D. & Bruce, P. G. Overcharging manganese oxides: Extracting lithium beyond Mn^{4+}. *J. Power Sources* **146**, 275–280 (2005).

67. Ohzuku, T., Nagayama, M., Tsuji, K. & Ariyoshi, K. High-capacity lithium insertion materials of lithium nickel manganese oxides for advanced lithium-ion batteries: toward rechargeable capacity more than 300 mA h g−1. *J. Mater. Chem.* **21**, 10179 (2011).

68. Jain, A. *et al.* Commentary: The materials project: A materials genome approach to accelerating materials innovation. *APL Mater.* **1**, 011002 (2013).

69. Ong, S. P., Wang, L., Kang, B. & Ceder, G. Li-Fe-P-O_2 Phase Diagram from First Principles Calculations. *Chem. Mater.* **77**, 1798–1807 (2008).

70. Jain, A. *et al.* Formation enthalpies by mixing GGA and GGA + U calculations. *Phys. Rev. B - Condens. Matter Mater. Phys.* **84**, 045115 (2011).

71. Strehle, B. *et al.* The Role of Oxygen Release from Li- and Mn-Rich Layered Oxides during the First Cycles Investigated by On-Line Electrochemical Mass Spectrometry. *J. Electrochem. Soc.* **164**, A400–A406 (2017).

72. Thackeray, M. M., Chan, M. K. Y., Trahey, L., Kirklin, S. & Wolverton, C. Vision for Designing High-Energy, Hybrid Li Ion/Li–O_2 Cells. *J. Phys. Chem. Lett.* **4**, 3607–3611 (2013).

73. Ruther, R. E., Callender, A. F., Zhou, H., Martha, S. K. & Nanda, J. Raman Microscopy of Lithium-Manganese-Rich Transition Metal Oxide Cathodes. *J. Electrochem. Soc.* **162**, A98–A102 (2014).

74. Thackeray, M. M. Manganese oxides for lithium batteries. *Prog. Solid State Chem.* **25**, 1–71 (1997).

75. Jansen, V. M. & Hoppe, R. Zur Kenntnis der NaCI-Strukturfamilie: Neue Untersuchungen an Li_2MnO_3. *Z. anorg. allg. Chem* **397**, 279–289 (1973).

76. Fischer, D., Hoppe, R., Schäfer, W. & Knight, K. S. Koordinationszahl 4 oder 6 für Lithium?: Die Kristallstruktur von wasserfreiem Lithiumpermanganat, Li[MnO_4]. *Z. Anorg. Allg. Chem.* **619**, 1419–1425 (1993).

77. Kitchaev, D. A. *et al.* Energetics of MnO_2 polymorphs in density functional theory. *Phys. Rev. B - Condens. Matter Mater. Phys.* **93**, 045132 (2016).

78. Chevrier, V. L., Ong, S. P., Armiento, R., Chan, M. K. Y. & Ceder, G. Hybrid density functional calculations of redox potentials and formation energies of transition metal compounds. *Phys. Rev. B* **82**, 075122 (2010).

79. Aykol, M., Dwaraknath, S. S., Sun, W. & Persson, K. A. Thermodynamic limit for synthesis of metastable inorganic materials. *Sci. Adv.* **4**, 1–8 (2018).

80. Chase Jr., M. W. *NIST-JANAF Thermochemical Tables*. (American Chemical Society, 1998).

81. Pauling, L. *The nature of the chemical bond and the structure of molecules and crystals : an*

introduction to modern structural chemistry. (Cornell University Press, 1960).

82. Zheng, J. *et al.* Electrochemical Kinetics and Performance of Layered Composite Cathode Material $Li[Li_{0.2}Ni_{0.2}Mn_{0.6}]O_2$. *J. Electrochem. Soc.* **160**, 2212–2219 (2013).

83. Yu, H.-C. *et al.* Designing the next generation high capacity battery electrodes. *Energy Environ. Sci.* **7**, 1760 (2014).

84. Li, V. Von & Hoppe, V. G. M. R. Zum thermischen Verhalten von Li_3MnO_4 I. [1]. Über α- und β-Li_3MnO_4. **266**, 249–256 (1976).

85. Ammundsen, B. *et al.* Local Structure and First Cycle Redox Mechanism of Layered $Li_{1.2}Cr_{0.4}Mn_{0.4}O_2$ Cathode Material. *J. Electrochem. Soc.* **149**, A431 (2002).

86. Balasubramanian, M., McBreen, J., Davidson, I. J., Whitfield, P. S. & Kargina, I. In Situ X-Ray Absorption Study of a Layered Manganese-Chromium Oxide-Based Cathode Material. *J. Electrochem. Soc.* **149**, A176 (2002).

87. Lu, Z. & Dahn, J. R. In Situ and Ex Situ XRD Investigation of $Li[Cr_xLi_{1/3-x/3}Mn_{2/3-2x/3}]O_2$ (x = 1/3) Cathode Material. *J. Electrochem. Soc.* **150**, A1044 (2003).

88. Na, Y., Ho, S., Chan, Y. & Bin, S. Characteristics of Li_2TiO_3-$LiCrO_2$ composite cathode powders prepared by ultrasonic spray pyrolysis. *J. Power Sources* **244**, 336–343 (2013).

89. Chalmin, E., Farges, F. & Brown, G. E. A pre-edge analysis of Mn K-edge XANES spectra to help determine the speciation of manganese in minerals and glasses. *Contrib. to Mineral. Petrol.* **157**, 111–126 (2009).

90. Van Schooneveld, M. M. & DeBeer, S. A close look at dose: Toward L-edge XAS spectral uniformity, dose quantification and prediction of metal ion photoreduction. *J. Electron Spectros. Relat. Phenomena* **198**, 31–56 (2015).

91. Garvie, L. A. J. & Craven, A. J. High-resolution parallel electron energy-loss spectroscopy of Mn $L_{2,3}$-edges in inorganic manganese compounds. *Phys. Chem. Miner.* **21**, 191–206 (1994).

92. Minasian, S. G. *et al.* Covalency in metal-oxygen multiple bonds evaluated using oxygen K-edge spectroscopy and electronic structure theory. *J. Am. Chem. Soc.* **135**, 1864–1871 (2013).

93. Kleiner, K. *et al.* Origin of high capacity and poor cycling stability of Li-rich layered oxides - A long-duration in situ synchrotron powder diffraction study. *Chem. Mater.* (2018). doi:10.1021/acs.chemmater.8b00163

94. Kiefer, W. & Bernstein, H. J. Rotating Raman Sample Technique for Colored Crystal Powders; Resonance Raman Effect in Solid KMnO 4. *Appl. Spectrosc.* **25**, 609–613 (1971).

95. Du, K. *et al.* Exploring reversible oxidation of oxygen in a manganese oxide. *Energy Environ. Sci.* **9**, 2575–2577 (2016).

96. Ben Yahia, M., Vergnet, J., Saubanère, M. & Doublet, M. L. Unified picture of anionic redox in Li/Na-ion batteries. *Nat. Mater.* **18**, 496–502 (2019).

97. Qiao, Y. *et al.* Reversible anionic redox activity in Na_3RuO_4 cathodes: A prototype Na-rich layered oxide. *Energy Environ. Sci.* **11**, 299–305 (2018).

98. Griffith, W. P. Infrared Spectra of Tetrahedral Oxyanions of the Transition Metals. *J. Chem. Soc. A*

1467–1468 (1966).

99. Kresse, G. & Hafner, J. Ab Initio Molecular Dynamics for Liquid Metals. *Phys. Rev. B* **47**, 558–561 (1993).

100. Kresse, G. & Hafner, J. Ab Initio Molecular-Dynamics Simulation of the Liquid-Metal-Amorphous-Semiconductor Transition in Germanium. *Phys. Rev. B* **49**, 14251–14269 (1994).

101. Kresse, G. & Furthmüller, J. Efficiency of Ab-Initio Total Energy Calculations for Metals and Semiconductors Using a Plane-Wave Basis Set. *Comput. Mater. Sci.* **6**, 15–50 (1996).

102. Kresse, G. & Furthmüller, J. Efficient Iterative Schemes for Ab Initio Total-Energy Calculations Using a Plane-Eave Basis Set. *Phys. Rev. B* **54**, 11169–11186 (1996).

103. Blöchl, P. E. Projector Augmented-Wave Method. *Phys. Rev. B* **50**, 17953 (1994).

104. Perdew, J. P., Burke, K. & Ernzerhof, M. Generalized Gradient Approximation Made Simple [Phys. Rev. Lett. 77, 3865 (1996)]. *Phys. Rev. Lett.* **78**, 1396 (1997).

105. Heyd, J., Scuseria, G. E. & Ernzerhof, M. Hybrid Functionals Based on a Screened Coulomb Potential. *J. Chem. Phys.* **118**, 8207 (2003).

106. Krukau, A. V, Vydrov, O. A., Izmaylov, A. F. & Scuseria, G. E. Influence of the Exchange Screening Parameter on the Performance of Screened Hybrid Functionals. *J. Chem. Phys.* **125**, 224106 (2006).

107. Dudarev, S., Botton, G., Savrasov, S., Humphreys, C. & Sutton, A. Electron-energy-loss spectra and the structural stability of nickel oxide: An LSDA+U study. *Phys. Rev. B* **57**, 1505–1509 (1998).

108. Blöchl, P., Jepsen, O. & Andersen, O. Improved tetrahedron method for Brillouin-zone integrations. *Phys. Rev. B* **49**, 16223–16233 (1994).

109. Chernova, N. A. *et al.* What can we learn about battery materials from their magnetic properties? *J. Mater. Chem.* **21**, 9865 (2011).

Supplementary Information for “Mn oxidation as the origin of the anomalous capacity of Mn-containing Li-excess cathode materials”

Maxwell D. Radin, Julija Vinckeviciute, Ram Seshadri, Anton Van der Ven
Materials Department
University of California Santa Barbara, Santa Barbara 93106-5050

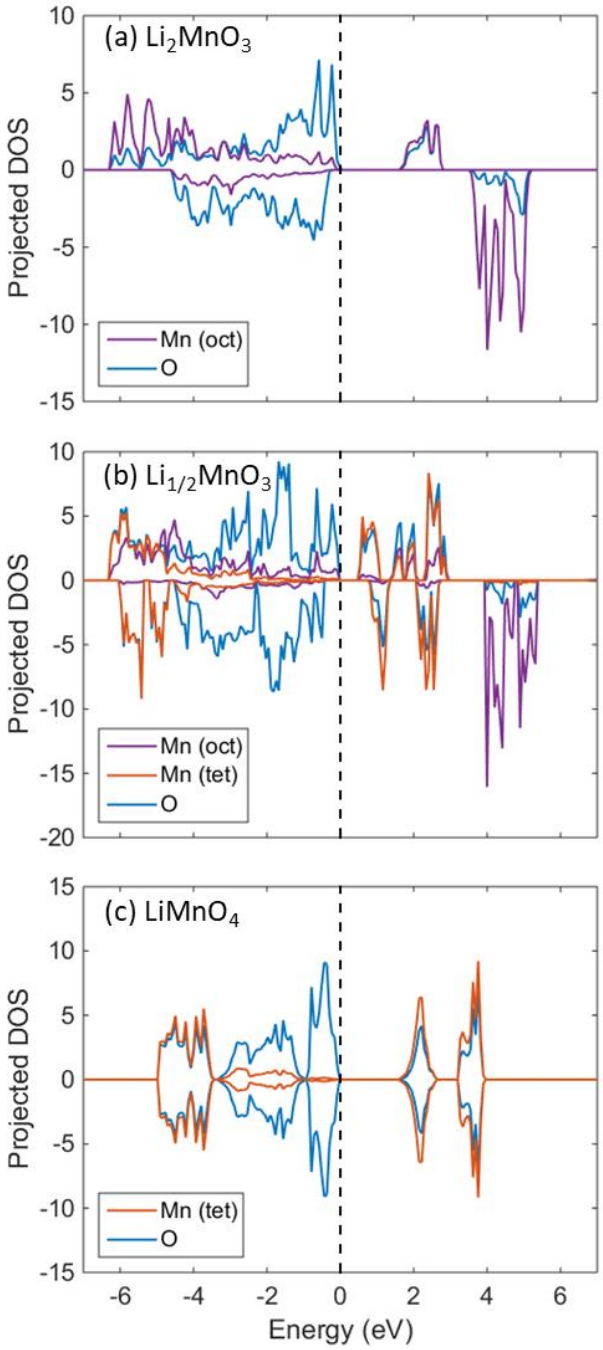

Supplementary Fig. 1. Comparison of the site-projected density of states (DOS) for the hypothesized $Li_{1/2}MnO_3$ structure to that of reference Mn^{4+} and Mn^{7+} compounds. a-c*, site-projected DOS (normalized per atom) of Li_2MnO_3, the hypothesized $Li_{1/2}MnO_3$ structure, and $LiMnO_4$, calculated with U = 5 eV. The dashed vertical line represents the valence band maximum. Comparing the purple lines in panels a and b shows that the site-projected DOS for octahedral Mn in $Li_{1/2}MnO_3$ is similar to that of Mn in Li_2MnO_3, confirming that the octahedral Mn sites can be interpreted as being in the +4 oxidation state. Comparing the red lines in panels b and c shows that the site-projected DOS for tetrahedral Mn in $Li_{1/2}MnO_3$ is similar to that of Mn in $LiMnO_4$ (aside from a rigid shift of ~1 eV), confirming that the tetrahedral Mn sites can be interpreted as being in the +7 oxidation state. This rigid shift can be understood as an artifact of the energies being plotted relative to the valence band maximum and do not represent a change in the qualitative nature of the electronic structure.*

Supplementary Table 1. Magnetic moments of Mn and O in the hypothesized $Li_{1/2}MnO_3$ structure and reference Mn^{4+} and Mn^{7+} compounds, calculated with U = 5 eV. *In structures with several symmetrically unique oxygen sites, Table 1 lists the minimum and maximum magnetic moment amongst all oxygen sites. The magnetic moments for $LiMn_2O_6$ are consistent with the octahedral Mn ions being in the +4 oxidation state and the tetrahedral Mn ions in the +7 oxidation state, with O ions remaining in the −2 state. The small but non-zero amount of magnetization on Mn^{7+} and O^{2-} sites can be understood as a consequence of hybridization.*

	Mn (octahedral)	Mn (tetrahedral)	O
$Li_{1/2}MnO_3$	3.461	0.215	-0.020, -0.257
Li_2MnO_3	3.271		-0.088, -0.097
$LiMnO_4$		0.000	0.000

Supplementary discussion

Comparison of calculated voltages for manganese oxidation and oxygen redox

In order to assess the relative thermodynamic favorability of manganese oxidation and oxygen redox, we calculated the energies of several structures representing delithiated Li_2MnO_3 in which the Mn remain in their original octahedral sites. Removal of Li in this manner results in the emptying of oxygen p-states.[1] We will refer to these structures as "oxygen redox structures". We enumerated and calculated all of the possible Li-vacancy orderings in a two-unit Li_2MnO_3 cell using PBE+*U*, HSE, and SCAN. We considered U = 3.9 eV and 5 eV, comparable to the values of U_{eff} that have previously been found to be suitable for manganese oxides.[2–4] In addition to the octahedral Li sites, we also included the two tetrahedral sites that face-share with the Li octahedral site in the transition-metal layer, although we only allowed the occupation of these sites if all of the adjacent octahedral sites were empty. The structures along the hull and a few at the $Li_{1/2}MnO_3$ composition were recalculated using HSE.

Supplementary Fig. 2 compares the thermodynamic stabilities of these oxygen redox structures to the $Li_{1/2}MnO_3$ structure depicted in Fig. 3 of the main text, in which half the Mn occupy tetrahedral sites. While PBE+*U* (U = 5 eV) predicts the $Li_{1/2}MnO_3$ structure with mixed tetrahedral/octahedral Mn to be above the convex hull (and therefore metastable with respect to the oxygen-redox structures), a value of U = 3.9 eV favors the mixed tetrahedral/octahedral Mn structure over the oxygen redox structures. Similarly, HSE and SCAN predict the mixed tetrahedral/octahedral Mn structure to have a lower energy than the oxygen-redox configurations considered.

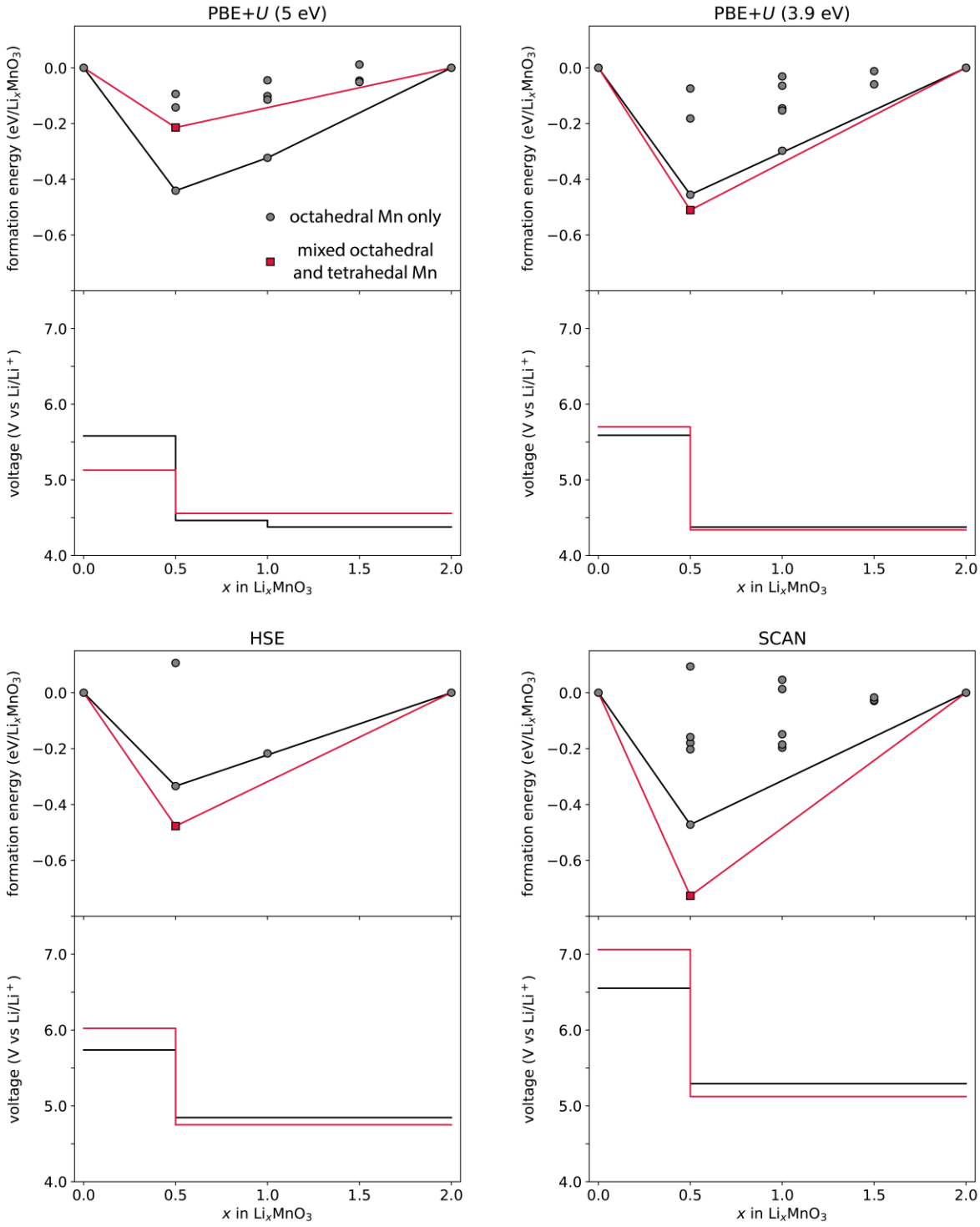

Supplementary Fig. 2. Comparison of formation-energy convex hulls and stable/metastable voltage curves calculated using PBE+U (U = 5 eV and 3.9 eV), HSE, and SCAN methods. *Grey points correspond to Li_xMnO_3 in which the Mn remain in their original octahedral sites (oxygen redox structures) while the red square is the energy of the proposed $Li_{1/2}MnO_3$ structure consisting of a mix of tetrahedral and octahedral Mn.*

An estimate of the uncertainties in first-principles calculations is central to interpreting the calculated voltages and phase stability. Benchmarks on Li-ion intercalation compounds show that both PBE+*U* (with the value of *U* obtained from linear-response theory) and HSE (with a mixing parameter $\alpha = 0.25$) can predict the voltages of lithium intercalation reactions based on 2+/3+ and 3+/4+ transition-metal redox couples to within a few tenths of a volt.[5] A striking example is the canonical Li-ion cathode material $LiCoO_2$, whose voltage is overestimated by 0.4 V with HSE with the standard mixing parameter of $\alpha = 0.25$.[5] It has been suggested that adjusting the mixing parameter to reproduce band gaps measured spectroscopically or predicted from GW calculations could yield more accurate intercalation voltages.[6]

The accuracy of first principles methods for intercalation voltages based on Mn^{4+}/Mn^{7+} and O^{2-}/O^{-} redox is not as well characterized as that of the 2+/3+ and 3+/4+ transition-metal redox couples. It has been suggested that HSE provides a more accurate description of oxygen redox than DFT+*U* because, unlike DFT+*U*, HSE corrects self-interaction error associated with oxygen p orbitals.[1] This notion is supported by our calculations, which show that HSE ($\alpha = 0.25$) predicts a higher voltage for oxygen redox than PBE+*U*.

Applying the notion that a hybrid functional is required for a correct description of oxygen redox to the results shown in Supplementary Fig. 2 suggests that manganese oxidation from Mn^{4+} to Mn^{7+} with concomitant migration from octahedral to tetrahedral coordination is thermodynamically favored. For example, if one were to assume that HSE ($\alpha = 0.25$) provided the correct voltages for both manganese oxidation and oxygen redox, then the voltage curves in Supplementary Fig. 2 would imply that manganese oxidation is favored. The same conclusion would be reached if one were to assume that HSE ($\alpha = 0.25$) provided the correct voltage for oxygen redox but PBE+*U* (*U* = 5 eV) provided the correct voltage for manganese oxidation. However, in light of the benchmarks on 2+/3+ and 3+/4+ redox couples (and the lack of benchmarks for the Mn^{4+}/Mn^{7+} and O^{2-}/O^{-} couples), we emphasize that the PBE+*U* and HSE results above do not allow for a definitive determination of whether oxygen redox or manganese oxidation is thermodynamically favored in the Li-excess manganese oxides.

Another challenge in relating the calculated and experimental voltages is that Mn migration potentially may be facile enough to permit Mn diffusion to be in or near equilibrium, at least on the nano scale. In this case, the voltage for manganese oxidation may be closer to that calculated for the three phase reactions in Eqs. 3-5. Similarly, facile Mn migration may cause the voltage for oxygen redox to be closer to that calculated for structures wherein Mn resides in the Li layer and where redox occurs on oxygen. Such structures have been previously predicted to be lower in energy (at the PBE+*U* level of theory) than "oxygen-redox structures" structures wherein the Mn stays in the transition-metal layer.[7]

Redox mechanisms in Ir and Ru oxides

A review of the literature shows that an activation process and hysteresis occur only in the Ru and Ir compounds that are expected to undergo octahedral/tetrahedral migration based on available information about the coordination preferences of Ru and Ir ions. Li_2RuO_3 exhibits a strong activation process and hysteresis when cycled over a capacity corresponding to an average Ru oxidation state that goes from +4 to approximately +5.5. This implies that some Ru ions would be oxidized to the +6 oxidation state or higher, which is likely to result in octahedral/tetrahedral migration: Ru^{4+} and Ru^{5+} oxides favor octahedral coordination[8,9] while Ru^{6+}, Ru^{7+}, and Ru^{8+} oxides are known to exhibit tetrahedral coordination.[10–12] Li_2IrO_3, in contrast, does not exhibit a strong activation process or hysteresis even when fully delithiated;[13,14] this is consistent with the fact that Ir^{4+}, Ir^{5+}, and Ir^{6+} oxides all favor octahedral coordination.[13,15,16] $Li_2Ir_{1/2}Sn_{1/2}O_3$[14] and Li_3IrO_4[17] on the other hand, exhibit strong activation processes

and hysteresis when cycled to capacities corresponding to average Ir oxidation states of approximately +7 and +7.5, respectively. Experiments have found that iridium oxide molecules and molecular ions wherein Ir is in the +7, +8, and +9 oxidation states exhibit tetrahedral coordination,[18,19] supporting the notion that the electrochemical oxidation of Ir beyond +6 may result in octahedral/tetrahedral migration. The electrochemical oxidation of Ir to oxidation states of +7 or higher would be remarkable because the preparation of Ir in such high oxidation states by conventional methods is challenging.

It is important to recognize that the electrochemical activity of pure Li_2IrO_3 had previously been hypothesized to arise from oxygen redox in the form of peroxo-like $(O_2)^{n-}$ species.[20,21] However, a recent Ir L-edge XANES study concluded that the electrochemical activity of this compound is best understood as arising from iridium oxidation (with some participation of oxygen due to covalency).[14] We emphasize that although the assignment of oxidation states to covalent compounds represents a simplifying approximation, oxidation states are nevertheless a profoundly useful tool in interpreting electronic structure.

Supplementary References

1. Seo, D. *et al.* The electronic origin of the oxygen redox activity in Li-excess cathode materials. *Nat. Chem.* **8**, 692–697 (2016).

2. Zhou, F., Cococcioni, M., Marianetti, C., Morgan, D. & Ceder, G. First-principles prediction of redox potentials in transition-metal compounds with LDA+U. *Phys. Rev. B* **70**, 235121 (2004).

3. Wang, L., Maxisch, T. & Ceder, G. Oxidation Energies of Transition Metal Oxides within the GGA+U Framework. *Phys. Rev. B* **73**, 195107 (2006).

4. Jain, A. *et al.* Formation enthalpies by mixing GGA and GGA + U calculations. *Phys. Rev. B - Condens. Matter Mater. Phys.* **84**, 045115 (2011).

5. Chevrier, V. L., Ong, S. P., Armiento, R., Chan, M. K. Y. & Ceder, G. Hybrid density functional calculations of redox potentials and formation energies of transition metal compounds. *Phys. Rev. B* **82**, 075122 (2010).

6. Seo, D. H., Urban, A. & Ceder, G. Calibrating transition-metal energy levels and oxygen bands in first-principles calculations: Accurate prediction of redox potentials and charge transfer in lithium transition-metal oxides. *Phys. Rev. B* **92**, 115118 (2015).

7. Lee, E. & Persson, K. A. Structural and Chemical Evolution of the Layered Li-Excess Li_xMnO_3 as a Function of Li Content from First-Principles Calculations. *Adv. Energy Mater.* **4**, 1400498 (2014).

8. Boman, C.-E. Refinement of the Crystal Structure of Ruthenium Dioxide. *Acta Chem. Scand.* **24**, 116–122 (1970).

9. Regan, K. A., Huang, Q. & Cava, R. J. Isolated spin 3/2 plaquettes in Na_3RuO_4. *J. Solid State Chem.* **178**, 2104–2108 (2005).

10. Fischer, D., Hoppe, R., Mogare, K. M. & Jansen, M. Syntheses, Crystal Structures and Magnetic Properties of Rb_2RuO_4 and K_2RuO_4. *Z. Naturforsch* **60**, 1113–1117 (2005).

11. Silverman, M. D. & Levy, H. A. Crystal Structure of Potassium Perruthenate, KRuO4. *J. Am. Chem. Soc.* **76**, 3317–3319 (1954).

12. Pley, M. & Wickleder, M. S. Two crystalline modifications of RuO4. *J. Solid State Chem.* **178**, 3209 (2005).

13. Pearce, P. E. *et al.* Evidence for anionic redox activity in a tridimensional-ordered Li-rich positive electrode β-Li_2IrO_3. *Nat. Mater.* **16**, 580–586 (2017).

14. Hong, J. *et al.* Metal–oxygen decoordination stabilizes anion redox in Li-rich oxides. *Nat. Mater.* doi:10.1038/s41563-018-0276-1

15. Bremholm, M., Dutton, S. E., Stephens, P. W. & Cava, R. J. $NaIrO_3$ - A pentavalent post-perovskite. *J. Solid State Chem.* **184**, 601–607 (2011).

16. Mugavero, S. J., Smith, M. D., Yoon, W. S. & zur Loye, H. C. $Nd_2K_2IrO_7$ and $Sm_2K_2IrO_7$: Iridium(VI) oxides prepared under ambient pressure. *Angew. Chem. Int. Ed.* **48**, 215–218 (2009).

17. Iro, L. *et al.* Approaching the limits of cationic and anionic electrochemical activity with the Li-rich layered. *Nat. Energy* **2**, 954–962 (2017).

18. Gong, Y., Zhou, M., Kaupp, M. & Riedel, S. Formation and Characterization of the Iridium Tetroxide Molecule with Iridium in the Oxidation State +VIII. *Angew. Chem. Int. Ed.* **48**, 7879–7883 (2009).

19. Wang, G. *et al.* Identification of an iridium-containing compound with a formal oxidation state of IX. *Nature* **514**, 475–478 (2014).

20. Assat, G. & Tarascon, J. Fundamental understanding and practical challenges of anionic redox activity in Li-ion batteries. *Nat. Energy* **3**, 373–386 (2018).

21. Grimaud, A., Hong, W. T., Shao-Horn, Y. & Tarascon, J. M. Anionic redox processes for electrochemical devices. *Nat. Mater.* **15**, 121–126 (2016).